Published in IET Renewable Power Generation
Received on 4th June 2009
Revised on 3rd December 2009
doi: 10.1049/iet-rpg.2009.0070

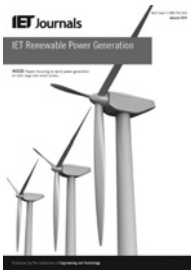

ISSN 1752-1416

Reliability assessment of a wind-power system with integrated energy storage

F.A. Bhuiyan A. Yazdani

University of Western Ontario, London, ON, Canada
E-mail: fbhuiyan@uwo.ca; ayazdani@eng.uwo.ca

Abstract: This study looks into reliability assessment and components rating of a wind-power system with integrated battery energy storage. The system can potentially be used in remote electrification projects to mitigate the reliance on diesel generators. A reliability assessment method has been proposed in this study, based on a combination of the traditional analytical and simulation-based approaches, to enable calculation of reliability indices, required battery capacity and power rating, and power rating of the power-electronic converter of the wind-power units. The proposed method is easy to implement in the MATLAB software environment, takes into account the units forced outage rate (FOR), and also permits modelling of the grid-connected mode.

Nomenclature

CSIG	constant-speed induction generator
DFIG	doubly-fed induction generator
WPSU	wind-power and storage unit
s_l	slip of DFIG
$f(.)$	probability density function
$F(.)$	cumulative distribution function
$p_r(.)$	probability of
v	wind speed, in m/s
i	subscript denoting the availability of a generator (1: available, 2: unavailable)
j	subscript denoting the wind-speed condition
$S_{1j}^{(k)}$	state in which generator k is in the wind-speed condition j and available
$S_{2j}^{(k)}$	state in which generator k is in the wind-speed condition j and unavailable
$P_{ij}^{(k)}$	power output of generator k, in kW, at state S_{ij}
P_{ij}	total power output, in kW, at state S_{ij}
P_{rot}	rotor power of DFIG, in kW
P_{bat}	battery power, in kW
P_{L}	load power, in kW
P_{Le}	effective load power, in kW
$P_{\text{ch-max}}$	maximum permissible charging battery power, in kW
$P_{\text{dch-max}}$	maximum permissible discharging battery power, in kW
P_{ex}	battery power available for export, in kW
E_{min}	minimum permissible battery stored energy, in kWh
E_{max}	maximum permissible battery stored energy, in kWh
T	sampling period, in hr (unity in this paper)

1 Introduction

Electrification of remote communities and islands remains a burden on many utility companies in Canada and worldwide. In Canada, there are around 300 remote communities that are not connected to the power system [1]. In Northern Ontario, alone, there are about 30 remote communities that are isolated from a utility grid, and their electricity is supplied exclusively by diesel generators [2]. Many other remote communities are connected to the power system via unreliable transmission lines that pass through rough terrains or forests and, thus, experience frequent downtime due to landslides or wildfire. Presently,

the state-of-the-art remote electrification technique is to utilise diesel generators, [1–3], due to their simplicity, ruggedness and acceptable reliability. However, diesel generators are rather inefficient and pollute the environment. Moreover, the transportation of diesel fuel can be costly and risky. Thus, a fair number of studies have been conducted on the subject of augmenting diesel-based electric power generation with renewable energy resources which may be potentially available in many such remote sites [4–10].

Infield *et al.* [4] investigate different wind/diesel/storage systems in terms of economic operation. Nayar *et al.* [5] discuss multiple system configurations and the economics associated with major system components of a solar/wind/diesel system, which also includes energy storage. In [6] the economic dispatch problem in wind–diesel hybrid systems is investigated, whereas [7] deals with the modelling and performance of a wind–diesel hybrid system based on an electronically coupled squirrel-cage asynchronous generator. In [8] an electronically controlled, variable-frequency, wind–diesel hybrid system has been proposed to improve the overall system efficiency. Lopes and Almeida [9] propose a stand-alone wind-power unit based on the asynchronous generator and a reduced-rating voltage-sourced converter (VSC). Bhuiyan and Yazdani [10] study the operation and control of a doubly-fed induction generator (DFIG)-based wind-power unit augmented with the battery energy storage to run in the islanded mode as well as the grid-connected mode of operation. The aforementioned body of the literature, however, primarily deals with the feasibility of hybrid systems from the control, configuration and economy viewpoints, and not the reliability criteria or component sizing requirements to fulfill a certain level of reliability.

This paper deals with the issues of reliability and components rating for the wind-power/storage system introduced in [10]. The idea in [10] has been to utilise battery energy storage in conjunction with a DFIG-based wind-power unit, to enhance the reliability and continuity of electric power supply to a remote site. The battery energy storage enables the wind-power unit to satisfy the load such that the network voltage and frequency remain regulated. The proposed system can run in the islanded mode, as well as the grid-connected mode of operation. The reliability assessment methodology presented in this paper combines the traditional simulation-based [11] and analytical [12] approaches, and with minor modifications is also applicable to different configurations of hybrid systems. The proposed method takes into consideration the forced outage rate (FOR) of the wind-power unit(s), the FOR of the transmission line, the battery capacity and required power handling capability, and the random natures of the wind and load. The proposed algorithm has been implemented in MATLAB software environment, and its application to the wind-power/storage system of [10] has been demonstrated.

2 Study system

Fig. 1 illustrates a simplified schematic diagram of the study wind-power/storage unit (WPSU), interfaced with a remote distribution network. The WPSU is based on a DFIG, which is controlled by the back-to-back connection of a rotor-side converter (RSC) and a grid-side converter (GSC); a battery bank is interfaced with the converters dc link [10]. Fig. 1 also shows that the distribution network embeds a constant-speed induction generator (CSIG)-based wind-power unit, an aggregate of local loads, and a switch that can establish or interrupt the connection between the distribution network and the grid. Hereinafter, the CSIG-based wind-power unit is referred to as the CSIG.

In Fig. 1, $P_{ij}^{(1)}$ and $P_{ij}^{(2)}$ signify the wind powers extracted by the WPSU and the CSIG, respectively; the total wind power, $P_{ij}^{(1)} + P_{ij}^{(2)}$, is denoted hereinafter by P_{ij}. In the islanded mode, the battery power, P_{bat}, is automatically controlled through a voltage/frequency regulation scheme, [10], to compensate for the difference between P_{ij} and the total load power, P_L. In the grid-connected mode, however, P_{bat} is an independent control variable to either charge the battery or deliver a pre-specified amount of power to the rest of the system.

3 Reliability of study system

Wind energy is stochastic in nature and, as such, is often characterised by means of probabilistic techniques [13]. Voorspools and D'Haeseleer [14] establish that probabilistic methods in power systems are preferred over deterministic methods, even for short-term reserve planning calculations. In power systems, two distinct probabilistic methods exist for the calculation of reliability indices [12]. These are: (i) the closed-form (or analytical) method and (ii) the simulation-based method [11]. Based on the analytical approach, [15–17], Weibull probability density function (pdf) and the corresponding cumulative distribution function (cdf) are usually employed to characterise the wind speed [18]. These functions, in conjunction with the turbine power/wind-speed characteristic function, [19–23], characterise the power output of a wind-power unit. The main shortcoming of the analytical approach is that it cannot readily take into account the chronological variations

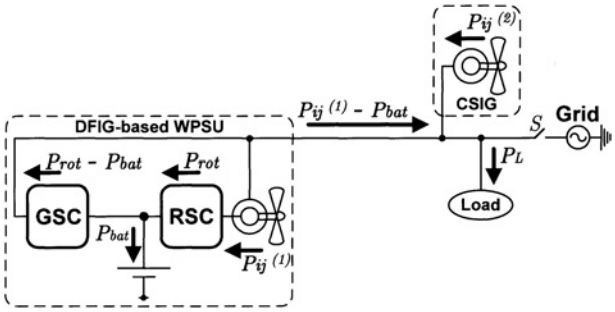

Figure 1 *Single line schematic diagram of the study system*

doi: 10.1049/iet-rpg.2009.0070

of the wind speed and the battery state-of-charge [24]. By contrast, in the simulation-based approach, wind speed is forecasted through a time-series analysis on the past wind data [25]. Although accurate, the simulation-based method requires a fairly complex forecast model and large amount of past wind data [26, 27].

In a number of investigations, wind and hybrid systems augmented with battery energy storage are modelled and analysed through probabilistic techniques [28, 29]. However, the reported studies do not consider the generators FOR and are limited to the islanded mode of operation. This paper proposes a new method for the calculation of the reliability indices based on a combination of the analytical and simulation-based approaches. The proposed hybrid method permits the use of a fairly limited volume of past wind data, for example for 1 year, and also takes into account the units FOR. The proposed method also accommodates the grid-connected mode of operation and enables the modelling of the battery state-of-charge. Although applied to a specific system configuration, the proposed method is also applicable to other system configurations.

3.1 Reliability index

In this paper, the loss of load expectation (LOLE) is considered as the reliability index. The LOLE is the expected duration within a certain period of time, for example, 1 year, over which the load demand exceeds the total generated power. Mathematically, the LOLE in hr/yr is expressed as

$$\begin{aligned}\text{LOLE} &= \sum_{h=1}^{n=8760} p_r((P_{ij}[h] - P_{Le}[h]) < 0) \\ &= \sum_{h=1}^{n=8760} p_r(P_{ij}[h] < P_{Le}[h]) \end{aligned} \quad (1)$$

where $P_{ij}[h]$ is the total generation during the hth hour and $n = 8760$ is the number of hours in a year. $P_{Le}[h]$ is the effective load power which is precisely defined in Section 3.2.

3.2 Proposed hybrid algorithm

The following algorithm is proposed in this paper for the calculation of the LOLE for the system of Fig. 1:

1. Hourly wind speeds of, for example, 1 year, expressed in the form of a time series, are input to the turbine(s) power/wind-speed characteristic function(s), and a time series is generated for the total power generation $P_{ij} = P_{ij}^{(1)} + P_{ij}^{(2)}$. To this end, steady-state power/wind-speed turbine characteristics [see (4)] may be employed since the sampling intervals are relatively long, that is $T = 1$ hr;

2. Based on either a load model or a set of hourly recorded data, a time series is constructed for the load power P_L;

3. Based on P_{ij}, P_L, and the control logic of the WPSU, the battery stored energy, E_{bat}, is calculated for all hours. Then, based on E_{bat}, the battery power available for export, P_{ex}, and subsequently the 'effective load power', $P_{\text{Le}} = P_{\text{L}} - P_{\text{ex}}$, are calculated for each hour and expressed in time-series forms; and

4. Using the 'capacity-in probability table', $p_r(P_{ij}[h] < P_{Le}[h])$ is calculated for each hour. Then, the hourly probabilities are integrated to calculate the LOLE, based on (1). The generators FORs take part in the construction of the capacity-in probability table.

3.2.1 Construction of time series for the total power generation: To construct the total power generation, hourly wind speed data, that is $v[h]$, is required. It is assumed in this paper that the data are available for at least 1 year and can be expressed as a time series. Using the time series and the turbine(s) power/wind-speed characteristic(s), the time series for the total power generation $P_{ij} = P_{ij}^{(1)} + P_{ij}^{(2)}$ can be constructed. In addition, a continuous pdf can be fitted on the time series to enable calculation of the probability of the wind speed to lie within a certain range. This probability is required for the construction of the capacity-in probability table, as further explained in Section 3.2.4. The most commonly adopted pdf for this purpose is the Weibull pdf [18]

$$f(v) = \frac{\beta}{\alpha}\left(\frac{v}{\alpha}\right)^{\beta-1} \exp\left[-\left(\frac{v}{\alpha}\right)^{\beta}\right] \quad (2)$$

where v is the wind speed in m/s. α and β are the pdf scale and shape parameters, respectively, and can be estimated using the wind speed time series. For the Weibull pdf, (2), the corresponding cdf is

$$\begin{aligned} F(V_0) &= p_r(v \le V_0) = \int_0^{V_0} f(\xi)\,\mathrm{d}\xi \\ &= 1 - \exp\left[-\left(\frac{V_0}{\alpha}\right)^{\beta}\right] \end{aligned} \quad (3)$$

which formulates the probability of the wind speed v being smaller than a value, V_0.

For each wind-power unit, the power output, $P_{ij}^{(k)}$, is calculated based on [19], as

$$P_{ij}^{(k)} = \begin{cases} 0 & \text{if } v < V_{\text{ci}} \text{ or } v > V_{\text{co}} \\ (a + bv + cv^2)P_{\text{rat}}^{(k)} & \text{if } V_{\text{ci}} \le v \le V_{\text{r}} \\ P_{\text{rat}}^{(k)} & \text{if } V_{\text{r}} \le v < V_{\text{co}} \end{cases} \quad (4)$$

where V_{ci}, V_{r}, and V_{co} are the cut-in, rated and cut-out wind speeds, respectively. $P_{\text{rat}}^{(k)}$ signifies the rated power output of the wind-power unit. The coefficients a, b and c can be calculated based on V_{ci} and V_{r}, as explained in [16] and [19]. The regulation of the power output at its rated value,

that is the third condition in (4), is fulfilled by a pitch-angle control scheme in a variable-speed unit, such as the WPSU, and by a stall regulation mechanism in a constant-speed unit, such as the CSIG.

It should be noted that the characteristic (4) is valid for a steady state regime, but adequate for the purpose of this paper due to the large sampling period (of $T = 1$ hr).

Equation (4) indicates that the power output is zero for wind speeds below V_{ci} or above V_{co}. Based on (4), the output power is held constant at $P_{rat}^{(k)}$ when the wind speed is between V_r and V_{co}; this is ensured by pitch-angle control in the WPSU or by stall control in the CSIG. Equation (4) further indicates that when the wind speed is between V_{ci} and V_r, the power output is a quadratic function of the wind speed.

3.2.2 Construction of time series for load power consumption: The simplest widely adopted load model is based on the hourly peak power consumption [12], and is constructed by recording the load peak power in a particular site, over, for example, 1 year. This model yields a fairly accurate representation of the load, since it also accounts for the seasonal load changes.

Alternatively, the load can be characterised by a pdf. Two commonly used pdfs are the uniform pdf and the normal pdf. For a uniformly distributed load, the pdf is

$$f(P_L) = \begin{cases} (P_{Lmax} - P_{Lmin})^{-1} & \text{if } P_{Lmin} \le P_L \le P_{Lmax} \\ 0 & \text{otherwise} \end{cases} \tag{5}$$

where P_{Lmax} is the maximum yearly load peak power, and P_{Lmin} is the minimum yearly load peak power. The pdf of a normally distributed load can be expressed as

$$f(P_L) = \frac{1}{\sqrt{2\pi\sigma^2}} e^{-(P_L - m/\sqrt{2}\sigma)^2} \tag{6}$$

where m is the mean value and σ is the standard deviation. Once the pdf is determined, the time series $P_L[h]$ can be generated by suitable MATLAB commands, based on (5) or (6). If the diurnal load variations are of prime importance, the IEEE reliability test system (IEEE-RTS) load model is often adopted. In this paper, the IEEE-RTS load model is constructed based on the method described in [11, 30].

Commonly, the hourly load peak power values are arranged in a descending order, and the resultant time series is referred to as the load duration curve (LDC) [11]. An LDC indicates the total number of hours in a year during which the load power is larger than a value on the vertical axis. To enable better comparisons, three LDCs corresponding to a hypothetical load are shown in Fig. 2. The load maximum and minimum yearly peak powers are

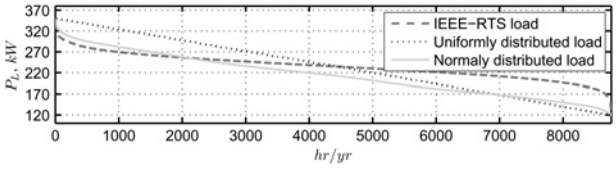

Figure 2 *LDCs corresponding to three different load models*

350 and 120 kW, respectively. The three LDCs of Fig. 2 are generated based on the IEEE-RTS model, (5) and (6), respectively.

3.2.3 Construction of time series for battery power, battery stored energy, and battery power available for export: Due to the variable natures of wind and load, in an off-grid system the power output of a wind-power unit does not necessarily match the load power. Therefore a battery (bank) is required to compensate for the power imbalance and to ensure voltage and frequency stability. The battery power is conditioned by the GSC of the WPSU, Fig. 1, and is controlled through a voltage/frequency regulation strategy [10].

In the islanded mode, the battery power is expressed as

$$P_{bat}[h] = \begin{cases} -P_{dch-max} & \text{if } P_{ij}[h] - P_L[h] \le -P_{dch-max} \\ P_{ij}[h] - P_L[h] & \text{if } -P_{dch-max} \le P_{ij}[h] - P_L[h] \le P_{ch-max} \\ P_{ch-max} & \text{if } P_{ij}[h] - P_L[h] \ge P_{ch-max} \end{cases} \tag{7}$$

where P_{ch-max} is the maximum power that can be delivered to the battery when it is being charged. $P_{dch-max}$ is the maximum power that can be drawn from the battery when it is being discharged; it is assumed in this paper that $0 < P_{dch-max} < P_{ch-max}$.

Based on the battery power, the battery stored energy (in kWh) is described by the following dynamic equation

$$E_{bat}[h+1] = \begin{cases} E_{min} & \text{if } E_{bat}[h] + TP_{bat}[h] \le E_{min} \\ E_{bat}[h] + TP_{bat}[h] & \text{if } E_{min} \le E_{bat}[h] + TP_{bat}[h] \le E_{max} \\ E_{max} & \text{if } E_{max} \le E_{bat}[h] + TP_{bat}[h] \end{cases} \tag{8}$$

where E_{min} and E_{max} are, respectively, the lower and upper limits of the battery stored energy, $E_{bat}[1] = E_{min}$, $T = 1$ hr is the sampling period, and $1 \le h \le 8760$. E_{min} and E_{max} impose major implications on the reliability of the system of Fig. 1.

As (7) indicates, the battery power $P_{bat} = P_{ij} - P_L$ must be limited from the upper side to the maximum value P_{ch-max}. This is ensured through rapid introduction of dump loads,

doi: 10.1049/iet-rpg.2009.0070

as well as a rather slow control of the DFIG pitch angle. P_{bat} must also be limited from the lower side to $-P_{dch-max}$. Thus, in case of inadequate generation, if the pitch angle of WPSU is already at its minimum, the loads may have to be dropped or the system be entirely shut down. The same measures are also taken if $E_{bat}[h+1]$ is either to exceed E_{max} or to become less than E_{min}.

The battery power available for export, P_{ex}, is defined as

$$P_{ex}[h] \triangleq \begin{cases} T^{-1}(E_{bat}[h]-E_{min}) & \text{if } T^{-1}(E_{bat}[h]-E_{min}) \le P_{dch-max} \\ P_{dch-max} & \text{if } T^{-1}(E_{bat}[h]-E_{min}) > P_{dch-max} \end{cases} \quad (9)$$

It should be noted that, unlike P_{bat}, P_{ex} is a positive mathematical variable which bears no physical meaning. P_{ex} represents the amount of power that can potentially be drawn from the battery if P_L exceeds P_{ij}. As (9) indicates, P_{ex} depends on E_{bat} and is limited to $P_{dch-max}$; its magnitude is such that the battery cannot be discharged to any level lower than E_{min}, in 1 hr.

3.2.4 Construction of the capacity-in probability table: FOR is the probability of a generator being out of service for a period of time [12]. Alternatively, 1−FOR is the probability of a generator being operational. Thus, the power output of a wind-power unit, as formulated by (4), depends not only on the wind condition, but also on the FOR. This is graphically illustrated by the state transition diagram of Fig. 3 where three states are identified as 'Down', 'Up1', and 'Up2'. The state 'Down' indicates that either the generator is out of service or the wind speed lies within the first piece of (4). 'Up1' and 'Up2' both represent a healthy generator. They, however, correspond to two different wind speed ranges; these are, respectively, (1) the wind speeds higher than V_{ci} but lower than V_r, and (2) the wind speeds higher than V_r but lower than V_{co}. Table 1 provides the states probabilities and the corresponding power outputs, based on the diagram of Fig. 3. The states are generically denoted by $S_{ij}^{(k)}$.

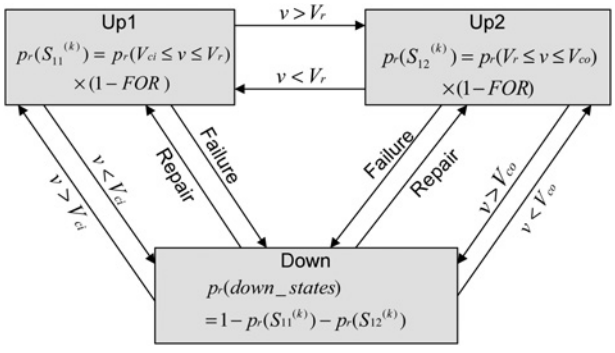

Figure 3 *State transition diagram for a wind-power unit without energy storage*

Table 1 States probabilities for generator k

State	State probability	Expected power output
$S_{11}^{(k)}$	$(1 - FOR) \times p_r(V_{ci} \le v \le V_r)$	$P_{11}^{(k)}$ (10)
$S_{12}^{(k)}$	$(1 - FOR) \times p_r(V_r \le v < V_{co})$	$P_{12}^{(k)} = P_{rat}^{(k)}$
$S_{13}^{(k)}$	$(1 - FOR) \times p_r(v < V_{ci} \cup v \ge V_{co})$	$P_{13}^{(k)} \equiv 0$
$S_{21}^{(k)}$	$FOR \times p_r(V_{ci} \le v \le V_r)$	$P_{21}^{(k)} \equiv 0$
$S_{22}^{(k)}$	$FOR \times p_r(V_r \le v \le V_{co})$	$P_{22}^{(k)} \equiv 0$
$S_{23}^{(k)}$	$FOR \times p_r(v < V_{ci} \cup v \ge V_{co})$	$P_{23}^{(k)} \equiv 0$

For $S_{ij}^{(k)}$, $k = 1$ corresponds to the WPSU, whereas $k = 2$ represents the CSIG. The subscript i represents the state-of-health of the generator in question. Thus, $i = 1$ represents a healthy corresponding generator, whereas $i = 2$ indicates that the generator is out of service. The subscript j corresponds to a wind-speed range, as identified in Table 2. Due to the three wind-speed conditions and states of health, each generator can assume any of the six states introduced in Table 1. A brief explanation on the construction of Table 1 follows.

Consider, for example, the states $S_{11}^{(k)}$ and $S_{12}^{(k)}$. These states indicate that the generator k is healthy and can potentially deliver power. For both states, the wind speed is in such a range that enables power generation. Now consider the state $S_{13}^{(k)}$; although in this state the generator is healthy, the power output is zero due to the wind speed range (see Table 2). In the states $S_{21}^{(k)}$, $S_{22}^{(k)}$ and $S_{23}^{(k)}$, the generator is out of service. Consequently, the power output is zero, irrespective of the wind-speed condition. In Table 1, the power output corresponding to the state $S_{ij}^{(k)}$ is denoted by $P_{ij}^{(k)}$. Thus, as Table 1 shows, a generator delivers power only if it is healthy and the wind speed is in an appropriate range.

The probability of each state is equal to the probability of the unit being healthy or unhealthy, multiplied by the probability of the wind-speed being within the corresponding range. For example, the probability of $S_{11}^{(k)}$ is the probability of the generator being up, that is 1-FOR, times $p_r(V_{ci} \le v \le V_r)$ which is calculated based on (3). As another example, the probability of $S_{22}^{(k)}$ is the probability of the generator being out of service, that is FOR, multiplied by $p_r(V_r \le v < V_{co})$, and so forth.

Table 2 Explanation of subscript j in $S_{ij}^{(k)}$ ($i = 1$ or 2)

j	Wind condition
1	$V_{ci} \le v \le V_r$
2	$V_r \le v < V_{co}$
3	$v < V_{ci}$ or $v \ge V_{co}$

If both WPSU and CSIG are considered, Table 1 can be expanded to Table 3 which includes all possible combinations of the states, their corresponding probabilities and their respective power outputs. It should be noted that since both generators are assumed to be subject to the same wind condition, for calculation of $p_r(S_{ij}^{(1)}$ and $S_{lj}^{(2)})$, the probability of the wind speed to be within a specific range appears as a first-order factor. However, the probability of the availability or unavailability of a generator is assumed to be independent of that of the other generator; the former probability is 1-FOR whereas the latter one is FOR.

If the elements of Table 3 are evaluated numerically and sorted in a descending order in terms of P_{ij}, the resultant table is referred to as the capacity-in probability table. The capacity-in probability table provides the probability of the generated power being less than or equal to a given value.

In constructing the numerical version of the capacity-in probability table, one complication is encountered. For each of the states $S_{11}^{(1)}$ and $S_{11}^{(2)}$, $S_{11}^{(1)}$ and $S_{21}^{(2)}$, and $S_{21}^{(1)}$ and $S_{11}^{(2)}$, the power output of the healthy unit(s), that is $P_{11}^{(k)}$, can assume any value(s) between zero and the unit(s) corresponding rated power(s), depending on the wind speed in that particular hour. Similarly, the probability of the wind speed to be equal to the wind speed in that hour must be computed. To resolve this complication, the wind-speed range $V_{ci} \le v \le V_r$ is divided into a number of equal intervals. Then, the average power corresponding to each interval is estimated as

$$P_{11}^{(k)} = \frac{1}{\Delta V}\int_{\eta}^{\eta+\Delta V} P_{rat}^{(k)}(a + b\xi + c\xi^2)\,d\xi \qquad (10)$$

where η marks the beginning of the interval and ΔV is the interval length. The probability of the wind speed being in the range $\eta \le v \le \eta + \Delta V$ is calculated based on (3) as

$$p_r(\eta \le v \le \eta + \Delta V) = \int_{\eta}^{\eta+\Delta V} f(\xi)\,d\xi = F(\eta + \Delta V) - F(\eta) \qquad (11)$$

In this paper, the range $V_{ci} \le v \le V_r$ is divided into four equal intervals. Therefore, the top three rows of Table 3, collectively, correspond to 12 rows of the numerical version of Table 3, which is reported in Section 5 as Table 4.

Table 3 State probabilities and corresponding power outputs for the system of Fig. 1

j	$S_{ij}^{(1)}$	$S_{lj}^{(2)}$	$p_r(S_{ij}^{(1)}$ and $S_{lj}^{(2)})$	expected total power output
1	$S_{11}^{(1)}$	$S_{11}^{(2)}$	$(1 - \text{FOR})^2 \times p_r(V_{ci} \le v < V_r)$	$P_{11}^{(1)} + P_{11}^{(2)}$
	$S_{11}^{(1)}$	$S_{21}^{(2)}$	$(1 - \text{FOR})(\text{FOR}) \times p_r(V_{ci} \le v < V_r)$	$P_{11}^{(1)}$
	$S_{21}^{(1)}$	$S_{11}^{(2)}$	$(\text{FOR})(1 - \text{FOR}) \times p_r(V_{ci} \le v < V_r)$	$P_{11}^{(2)}$
	$S_{21}^{(1)}$	$S_{21}^{(2)}$	$(\text{FOR})^2 \times p_r(V_{ci} \le v < V_r)$	0
2	$S_{12}^{(1)}$	$S_{12}^{(2)}$	$(1 - \text{FOR})^2 \times p_r(V_r \le v < V_{co})$	$P_{12}^{(1)} + P_{12}^{(2)} = P_{rat}^{(1)} + P_{rat}^{(2)}$
	$S_{12}^{(1)}$	$S_{22}^{(2)}$	$(1 - \text{FOR})(\text{FOR}) \times p_r(V_r \le v < V_{co})$	$P_{12}^{(1)} = P_{rat}^{(1)}$
	$S_{22}^{(1)}$	$S_{12}^{(2)}$	$(\text{FOR})(1 - \text{FOR}) \times p_r(V_r \le v < V_{co})$	$P_{12}^{(2)} = P_{rat}^{(2)}$
	$S_{22}^{(1)}$	$S_{22}^{(2)}$	$(\text{FOR})^2 \times p_r(V_r \le v < V_{co})$	0
3	$S_{13}^{(1)}$	$S_{13}^{(2)}$	$(1 - \text{FOR})^2 \times p_r(v_r < V_{ci}$ and $v > V_{co})$	0
	$S_{13}^{(1)}$	$S_{23}^{(2)}$	$(1 - \text{FOR})(\text{FOR}) \times p_r(v < V_{ci}$ and $v > V_{co})$	0
	$S_{23}^{(1)}$	$S_{13}^{(2)}$	$(\text{FOR})(1 - \text{FOR}) \times p_r(v < V_{ci}$ and $v > V_{co})$	0
	$S_{23}^{(1)}$	$S_{23}^{(2)}$	$(\text{FOR})^2 \times p_r(v < V_{ci}$ and $v > V_{co})$	0

Table 4 Numerical version of the capacity-in probability table of Table 3

γ	$p_r(P_{ij} = \gamma)$	$p_r(P_{ij} \le \gamma)$
2051	0.0974	1.0000
1678	0.0051	0.9026
1609	0.0979	0.8975
1316	0.0052	0.7995
872	0.1487	0.7944
714	0.0078	0.6457
373	0.0051	0.6378
360	0.1883	0.6327
294	0.0099	0.4444
292	0.0052	0.4345
158	0.0078	0.4293
70	0.1910	0.4215
65	0.0099	0.2305
57	0.0101	0.2206
12	0.0101	0.2106
0	0.2005	0.2005

doi: 10.1049/iet-rpg.2009.0070

4 WPSU GSC rating

In a conventional DFIG-based wind-power unit, the RSC and GSC handle a relatively small fraction of the DFIG electric power, approximately proportional to the DFIG slip and roughly limited to less than about 30% of the DFIG rated power. Although in the WPSU of Fig. 1 the rating of the RSC is the same as that in a conventional counterpart, the rating of the GSC may need to be considerably larger than due to both the battery and rotor power flows, Fig. 1.

The rotor power can be expressed in terms of the power output $P_{ij}^{(1)}$ as

$$P_{\text{rot}} = \frac{s_l}{1+s_l} P_{ij}^{(1)} \tag{12}$$

where s_l signifies the DFIG slip and is related to $P_{ij}^{(1)}$ as

$$s_l = \begin{cases} -1 + \sqrt[3]{K P_{ij}^{(1)}} & \text{if} \quad V_{\text{ci}} \le v \le V_{\text{co}} \\ \text{do not care otherwise} \end{cases} \tag{13}$$

where K is a constant. Fig. 4 illustrates the patterns of variation of s_l, P_{rot} and $P_{ij}^{(1)}$, for the WPSU when the wind speed changes from about 4–20 m/s, and $K = 1.309 \times 10^{-3}$ 1/(kW).

Equations (12) and (13) enable the construction of a time series for P_{rot}. The time series for P_{rot} is, in turn, used to construct a time series for the GSC power, as

$$P_{\text{GSC}}[h] = P_{\text{rot}}[h] - P_{\text{bat}}[h] \tag{14}$$

where $P_{\text{bat}}[h]$ is given by (7). Equation (14) indicates that P_{GSC} is composed of two counteracting components. To appreciate this, assume that the wind speed is large at some hours. This results in a large output power P_{ij}. Thus, the DFIG rotor power is positive and relatively large [(12) and (13), Fig. 4]. On the other hand, the large power generation most likely exceeds the load and, thus, results in a positive large value of P_{bat}. Consequently, the effect of large P_{rot} in P_{GSC} is outweighed. The same conclusions can also be made for a condition where the wind speed and the power output are low. The effect described above is desirable since it is in favour of a lower capacity GSC.

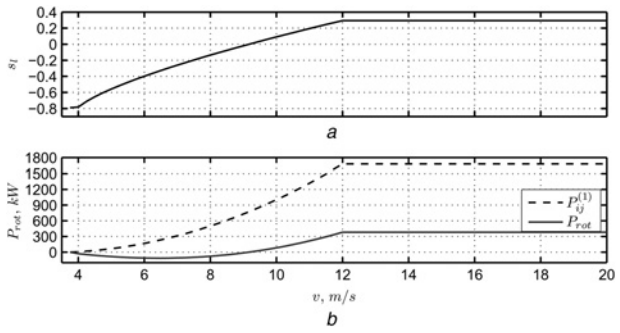

Figure 4 *Variations*

a Slip power as function of the wind speed
b Rotor power as function of the wind speed

5 Simulation results

The algorithm described in the previous sections has been implemented in the MATLAB software environment. The capacities of the WPSU and the CSIG are $P_{\text{rat}}^{(1)} = 1678$ kW and $P_{\text{rat}}^{(2)} = 373$ kW, respectively. To simplify the calculations, without loss of generality, both wind-power units are assumed to have the cut-in, rated, and cut-out wind speeds of 3.75, 12 and 23.2 m/s, respectively. The numerical values for the coefficients a, b and c are 0.1203, −0.08 and 0.0128, respectively. The other parameters are as follows, unless otherwise mentioned:

The wind-speed data are obtained from Environment Canada [31]. The data are recorded in the year 2007, in Argentia (AUT), Newfoundland. The same data is also used to specify the parameters of Weibull pdf as $\alpha = 8.0231$ and $\beta = 1.9852$. For the load power, an IEEE-RTS load model has been constructed [12, 30], that corresponds to the minimum and maximum yearly peak power values of, respectively, 120 and 350 kW, Fig. 2. For the batteries, $P_{\text{ch-max}} = 800$ kW, $P_{\text{dch-max}} = 350$ kW and $E_{\text{min}} = 0.05E_{\text{max}}$. For both the WPSU and the CSIG, FOR = 3%. However, FOR = 0 for the battery and the GSC. Table 4 is the numerical version of the capacity-in probability table of Table 3 and used for calculation of the LOLE. In Table 4, γ is a dummy variable expressed in kW. For example, assume that $P_{\text{Le}}[h] = 720$ kW at a given hour. Since $p_r(P_{ij}[h] \le \gamma) = 0.6457$ for $\gamma = 714$ (based on Table 4), then $p_r(P_{ij}[h] \le P_{Le}[h]) \simeq 0.6457$. This process can be repeated for all values of $P_{Le}[h]$ in a year, and the LOLE be determined based on (1).

5.1 Case 1: Impact of units FOR on the LOLE

The impact of the battery capacity E_{max} on the LOLE, for different values of FOR, is illustrated in Fig. 5. It is observed that, as expected, without battery the LOLE is prohibitively large. However, it decreases with the increase of E_{max}; for values beyond about 30 000 kWh, the LOLE is relatively small and any further increase in E_{max} does not result in a substantially lower LOLE. Fig. 5 also indicates that a higher FOR corresponds to a higher LOLE, for a given battery capacity. This impact, however, becomes less pronounced as the battery capacity is increased.

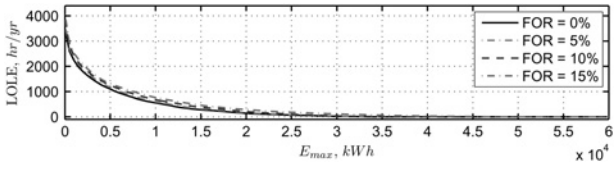

Figure 5 *Variations of LOLE against battery capacity, for different FOR*

5.2 Case 2: Impact of load distribution and maximum yearly peak power on the LOLE

The load distribution can have an appreciable impact on the LOLE against E_{max} curve. Fig. 6*a* illustrates the curves corresponding to the three different load distributions of Fig. 2. Fig. 6*a* indicates that while the LOLE exhibits very similar patterns of variation for the normal- and uniform-distributed loads, for a given E_{max}, the LOLE is the lowest for the IEEE-RTS load.

Fig. 6*b* shows the LOLE against E_{max} curves for three IEEE-RTS loads of different yearly maximum peak power values. It is observed that, expectedly, the LOLE increases as the load maximum peak power increases. However, the impact is relatively small for adequately large battery capacities, for example larger than 24 000 kWh.

5.3 Case 3: Impact of wind profile and magnitude on the LOLE

The methodology presented in this paper takes advantage of year-round wind-speed data. However, the wind profile is invariably different from year to year. Fig. 7*a* illustrates that the LOLE against E_{max} curves based on the wind-speed data of the years 2005 and 2007 are remarkably different. However, the impact become negligible if the battery capacity is adequately large, for example larger than 24 000 kWh.

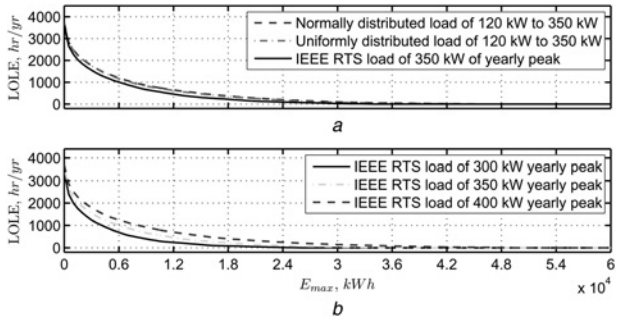

Figure 6 *LOLE against E_{max} curves*

a For different load distributions
b For different load yearly peak powers

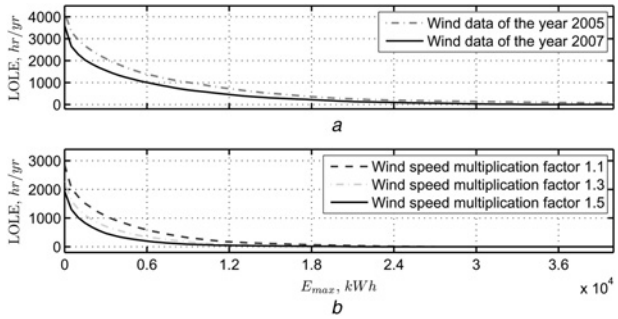

Figure 7 *LOLE against E_{max} curves*

a For different wind-speed time series
b For different wind-speed magnitudes

Fig. 7*b* demonstrates the effect of the wind strength on the LOLE against E_{max} curve. To run this simulation, the wind-speed time series of the year 2007 has been scaled by factors of 1.1, 1.3 and 1.5. Fig. 7*b* shows that, as expected, for a given battery capacity the LOLE becomes lower as the scale factor becomes larger. However, the impact becomes negligible at adequately large battery capacities, for example larger than 24 000 kWh.

5.4 Case 4: Impact of maximum permissible battery power on the LOLE

This case study demonstrates the impact of the maximum permissible battery charging and discharging rates, that is P_{ch-max} and $P_{dch-max}$, on the LOLE against E_{max} curves. Fig. 8*a* indicates that for a given E_{max}, the LOLE decreases as P_{ch-max} is increased. The reason is that a higher P_{ch-max} enables a faster battery charging which, in turn, ensures that more energy would be stored in the battery to be dispatched, if at any subsequent hour the load exceeds the generation. A higher P_{ch-max} translates into a higher-capacity GSC to handle the battery power and, therefore, should be chosen as the lowest value that fulfills the LOLE requirements.

Similarly, Fig. 8*b* indicates that, for a given battery capacity, the LOLE drops as $P_{dch-max}$ is increased. The impact of $P_{dch-max}$ on the LOLE is direct. The reason is that $P_{dch-max}$ corresponds to the maximum power that can be drawn from the battery, if the load exceeds the generation; this is apparent from (9). $P_{dch-max}$ can be assigned any value between zero and P_{ch-max}. However, its optimum value is expected to be slightly larger than the load maximum yearly peak power (350 kW in this paper).

5.5 Case 5: Impact of grid FOR on the LOLE

The system of Fig. 1 can also operate in the grid-connected mode [10]. Therefore it is worthwhile studying the impact

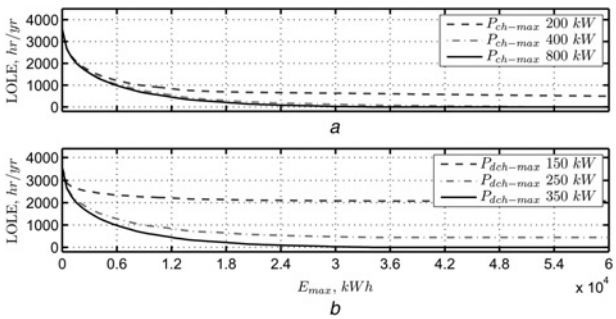

Figure 8 *LOLE against E_{max} curves*

a For $P_{dch-max}$ = 350 kW and different values of P_{ch-max}
b For P_{ch-max} = 800 kW and different values of $P_{dch-max}$

doi: 10.1049/iet-rpg.2009.0070

of the grid FOR on the LOLE. Fig. 9*a* illustrates three LOLE against E_{max} curves that correspond to different values of the grid FOR. Fig. 9*b* also illustrates a curve that corresponds to a grid FOR of 15% with the assumption that the grid downtime includes a continuous 96-h period. Fig. 9 indicates that, for a given battery capacity, the LOLE increases with the increase of FOR. Moreover, for a given FOR, the LOLE is higher if the downtimes are continuous.

A comparison between Figs. 9 and 5 indicates that the required battery capacity is considerably smaller in the grid-connected mode, as compared to the the islanded mode, even if the grid is fairly unreliable.

5.6 Case 6: GSC rating

$P_{GSC}[h]$ is the power that flows through the GSC, at the given hour. Thus the absolute value of $P_{GSC}[h]$ corresponds to the magnitude of power that the GSC must be able to handle in the hth hour. To obtain an idea about the required GSC power rating, the absolute values of $P_{GSC}[h]$ are sorted in a descending order and plotted against the hour axis. The resultant curve is shown in Fig. 10 and can be interpreted in a way similar to an LDC (Fig. 2). Thus, Fig. 10 indicates the total number of hours during which the GSC power is larger than a certain value on the vertical axis. For our system of study, Fig. 10 shows that the GSC power is always lower than about 800 kW. This result is consistent with the discussion of Section 4 that the maximum value of $|P_{GSC}|$ is about the same as P_{ch-max}. However, it will be remembered that, in determining the kVA rating of the GSC, the reactive power that this converter exchanges with the rest of the system must also be taken into consideration.

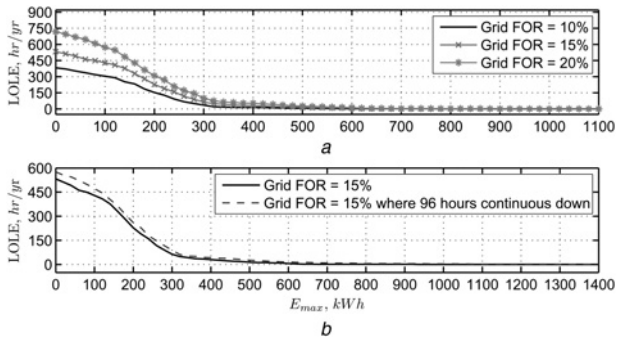

Figure 9 *LOLE against E_{max} curves in the grid-connected mode*

a For different values of the grid FOR
b For FOR = 15% totally random and FOR = 15% with 96 h continuous down

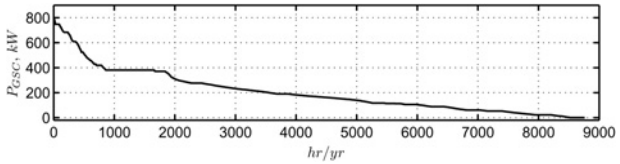

Figure 10 *Curve indicating the total number of hours per year during which the GSC power exceeds a certain value on the vertical axis*

6 Conclusions

Based on a new reliability assessment method, the reliability of a hypothetical wind-power system augmented with an integrated energy storage device was evaluated. It was shown that many parameters impact the system reliability. Among those, the wind strength plays a significant role. However, the battery capacity plays the most crucial role; the impact of all other parameters become negligible at an adequately large battery capacity. It was also discussed that the battery maximum discharging power should be chosen slightly higher than the expected maximum load peak power. However, provided the battery is properly rated, the maximum charging power can be assigned a considerably larger value, to ensure rapid energy storage and higher reliability. It was further shown that the operation in the grid-connected mode results in a considerably higher reliability, for a given battery capacity, even if the grid is fairly unreliable. The minimum battery size, the converter rating and the expected system reliability, determined by the proposed analysis method, should be viewed as reasonable estimates when a wind-power system with energy storage is planned; they may need to be refined for an installed system.

7 References

[1] AYOUB J., HENDERSON S., ALWARD R., SHERIFF F.: 'Living off-grid on renewable energy in the Yukon'. SESCI 2004 Conf., Waterloo, Canada, August 2004, pp. 1–12. Available at http://canmetenergy.nrcan.gc.ca/fichier.php/codectec/En/2004-128/2004-128e.pdf

[2] Hydro One Inc., (online). Available at http://www.hydroone.com

[3] KATIRAEI F., ABBEY C.: 'Diesel plant sizing and performance analysis of a remote wind-diesel microgrid'. IEEE Power Engineering Society General Meeting, PES 2007, Tampa, USA, June 2007, pp. 1–8

[4] INFIELD D.G., SLACK G.W., LIPMAN N.H., MUSGROVE P.J.: 'Review of wind/diesel strategies', *IEE Proc.*, 1983, **130**, (9), pp. 613–619

[5] NAYAR C.V., LAWRANCE W.B., PHILLIPHS S.J.: 'Solar/wind/diesel hybrid energy systems for remote areas'. 24th Intersociety Energy Conversion Engineering Conf., IECEC 89, Washington, DC, USA, August 1989, pp. 2029–2034

[6] CHAMBERS T.V., MUTALE J.: 'Selection of diesel generators for small rural wind-diesel power systems'. 41st Int.

Universities Power Engineering Conf., UPEC 06, Newcastle, UK, September 2006, pp. 51–55

[7] KINI A.S., YARAGATTI U.R.: 'Modeling and simulation of a wind/diesel hybrid power systems'. IEEE Int. Conf. on Industrial Technology, ICIT 06, Mumbai, India, December 2006, pp. 1670–1675

[8] SCOTT P.A., MUELLER M.A.: 'Modeling fully variable speed hybrid wind-diesel systems'. 41st Int. Universities Power Engineering Conf., UPEC 06, Newcastle, UK, September 2006, pp. 212–216

[9] LOPES L.A.C., ALMEIDA R.G.: 'Wind-driven self-excited induction generator with voltage and frequency regulated by a reduced-rating voltage source inverter', *IEEE Trans. Energy Convers.*, 2006, **21**, (2), pp. 297–304

[10] BHUIYAN F.A., YAZDANI A.: 'Multi-mode control of a DFIG-based wind-power unit for remote applications', *IEEE Trans. Power Deliv.*, 2009, **24**, (4), pp. 2079–2089

[11] BILLINTON R., ALLAN R.N.: 'Reliability evaluation of engineering systems' (Plenum Press, New York, 1992)

[12] BILLINTON R., ALLAN R.N.: 'Reliability evaluation of power systems' (Plenum Press, New York, 1996)

[13] BAKIRTZIS A.G.: 'A probabilistic method for the evaluation of the reliability of stand alone wind energy systems', *IEEE Trans. Energy Convers.*, 1992, **7**, (1), pp. 99–107

[14] VOORSPOOLS K.R., D'HAESELEER W.D.: 'Are deterministic methods suitable for short term reserve planning?', *J. Energy Convers. Manag.*, 2005, **46**, (13–14), pp. 2042–2052

[15] EHSANI A., FOTUHI M., ABBASPOUR A., RANJBAR A.M.: 'An analytical method for the reliability evaluation of wind energy systems'. IEEE Int. Region 10 Conf., TENCON 05, Melbourne, Australia, November 2005, pp. 1–7

[16] CHOWDHURY A.A.: 'Reliability models for large wind farms in generation system planning'. IEEE Power Engineering Society General Meeting, San Francisco, USA, June 2005, pp. 1926–1933

[17] LIU X., ISLAM S.: 'Reliability evaluation of a wind-diesel hybrid power system with battery bank using discrete wind speed frame analysis'. Ninth Int. Conf. on Probabilistic Method Applied to Power Systems, Stockholm, Sweden, June 2006, pp. 1–7

[18] MASTERS G.M.: 'Renewable and efficient electric power systems' (Wiley, New Jersey, 2004)

[19] GIORSETTO P., UTSUROGI K.F.: 'Development of a new procedure for reliability modeling of wind turbine generators', *IEEE Trans. Power Appar. Syst.*, 1983, **PAS-102**, (1), pp. 134–143

[20] ABOUZAHR I., RAMAKUMAR R.: 'Loss of power supply probability of stand-alone wind electric conversion systems: a closed form solution approach', *IEEE Trans. Energy Convers.*, 1990, **5**, (3), pp. 445–452

[21] ABOUZAHR I., RAMAKUMAR R.: 'An approach to assess the performance of utility-interactive wind electric conversion systems', *IEEE Trans. Energy Convers.*, 1991, **6**, (4), pp. 627–638

[22] SARAMOURTSIS A.C., BAKIRTZIS A.G., DOKOPOULOS P.S., GAVANIDOU E.S.: 'Probabilistic evaluation of performance of wind-diesel energy systems', *IEEE Trans. Energy Convers.*, 1994, **9**, (4), pp. 743–752

[23] KARAKI S.H., CHEDID R.B.: 'Probabilistic performance assessment of wind energy conversion systems', *IEEE Trans. Energy Convers.*, 1999, **14**, (2), pp. 217–224

[24] BILLINTON R., BAGEN , CUI Y.: 'Reliability evaluation of small stand-alone wind energy conversion systems using a time series simulation model', *IEE Proc. Gener. Transm. Distrib.*, 2003, **150**, (1), pp. 96–100

[25] BILLINTON R., CHEN H., GHAJAR R.: 'Time-series models for reliability evaluation of power systems including wind energy', *J. Microelectron. Reliab.*, 1996, **36**, (9), pp. 1253–1261

[26] KARKI R., HU P., BILLINTON R.: 'A simplified wind power generation model for reliability evaluation', *IEEE Trans. Energy Convers.*, 2006, **21**, (2), pp. 533–540

[27] KARKI R., HU P., BILLINTON R.: 'Reliability evaluation of a wind power delivery system using an approximate wind model'. 41st Int. Universities Power Engineering Conf., UPEC 06, Newcastle, UK, September 2006, pp. 113–117

[28] BOROWY B.S., SALAMEH Z.M.: 'Methodology for optimally sizing the combination of a battery bank and PV array in a wind/PV hybrid system', *IEEE Trans. Energy Convers.*, 1996, **11**, (2), pp. 367–375

[29] GHALI F.M.A., AZIZ M.M.A., SYAM F.A.: 'Simulation and analysis of hybrid systems using probabilistic techniques'. Power Conversion Conf., Naqaoka, Japan, August 1997, pp. 831–835

[30] ALBRETCH P.F.: TEST SYSTEM TASK FORCE: 'IEEE reliability test system', *IEEE Trans. Power Appar. Syst.*, 1979, **PAS-98**, (6), pp. 2047–2054

[31] (Online). Available at http://www.climate.weatheroffice.ec.gc.ca

doi: 10.1049/iet-rpg.2009.0070